



CHORUS

This is the accepted manuscript made available via CHORUS. The article has been published as:

Truncated Wigner dynamics and conservation laws

Peter D. Drummond and Bogdan Opanchuk

Phys. Rev. A **96**, 043616 — Published 18 October 2017

DOI: [10.1103/PhysRevA.96.043616](https://doi.org/10.1103/PhysRevA.96.043616)

Truncated Wigner dynamics and conservation laws

Peter D. Drummond and Bogdan Opanchuk

Centre for Quantum and Optical Science, Swinburne University of Technology, Melbourne 3122, Australia

Ultra-cold Bose gases can be used to experimentally test many-body theory predictions. Here we point out that both exact conservation laws and dynamical invariants exist in the topical case of the one-dimensional Bose gas, and these provide an important validation of methods. We show that the first four quantum conservation laws are exactly conserved in the approximate truncated Wigner approach to many-body quantum dynamics. Center-of-mass position variance is also exactly calculable. This is nearly exact in the truncated Wigner approximation, apart from small terms that vanish as $N^{-3/2}$ as $N \rightarrow \infty$ with fixed momentum cutoff. Examples of this are calculated in experimentally relevant, mesoscopic cases.

I. INTRODUCTION

We analyze conservation laws and exact dynamical results for the one-dimensional (1D) Bose gas, and use them to evaluate the accuracy of an approximate technique for quantum dynamics, the truncated Wigner equation [1, 2]. This is relevant to the topical case of soliton breather quantum fragmentation, which is an exponentially complex dynamical problem that can be tested in BEC experiments [3–6]. More generally, it shows that such phase-space methods may be more precise than expected, owing to the fact that they are able to maintain many of the symmetries and conservation laws of the underlying Heisenberg equations. In this case, dynamical evolution is constrained by local conservation laws [7, 8]. All four local conservation laws are exactly conserved in the truncated Wigner method, widely used in treating BEC dynamics [9, 10].

Quantum center-of-mass (COM) position spreading is another exact result [11, 12]. This is known to occur in photonic systems, although primarily due to amplifier or Raman noise [13]. It has been treated with the truncated Wigner method [14]. There are recent claims that this approximation exactly replicates quantum center-of-mass position spreading [15, 16]. We find that while the errors are small, this result is not exact. There is a small error in the position variance that scales as $1/N^{3/2}$ for N bosons. This is still much smaller than with some variational methods [3], where large errors occur [4] if too few natural modes are used.

We remark here that all closed quantum systems have large numbers of conserved observables, which we denote $\hat{H} = (\hat{H}_0, \hat{H}_1, \dots)$. These are linear combinations of the projection operators for the energy eigenstates. Some of these are simpler than others. For example, the conservation laws that arise from Noether's theorem [17] in quantum field theory are spatial integrals of local products of field operators and their derivatives. The most common examples of these are the particle number, the energy, and the momentum, but there is a fourth local conservation law in one-dimensional Bose gases. As well as determining the initial ensemble, such conserved quantities can be used to estimate the accuracy of approximate theories of quantum many-body time evolution [2, 9, 18, 19].

Since quantum field theories are exponentially complex, exact results allow estimation of errors in a way not feasible through other means.

Conserved quantities can allow further exact dynamical results to be obtained. One example that we use here is quantum center-of-mass motion. This can be treated using quantum phase-space methods [14]. Systems with distributions of particle number can also be analyzed [20]. More generally, other dynamical results may be available as well. Such results generally depend on the symmetries of the problem.

There is a more fundamental significance of these issues. The existence of infinite numbers of conservation laws means that the equilibrium density matrix can have a more general form than the usual Gibbs ensemble [21]. The most general form is an arbitrary function of the conserved operators, $\hat{\rho} = G(\hat{H})$. This is also related to a paradox raised by Feynman: the von Neumann quantum entropy is time-invariant in a closed system [22]. From a Bayesian viewpoint thermal ensembles simply express one's ignorance of the conservation laws. The more general equilibrium ensembles that must exist are not widely observed, owing to the difficulty of measuring and calculating higher conservation laws.

As a general rule, BEC experiments generically involve relatively short time dynamics, mixed states with variable particle number, finite temperature, decoherence and non-integrable perturbations. This makes it essential to have rather general theoretical strategies, such as the truncated Wigner technique described and evaluated here. Despite this, it is instructive to examine idealized non-dissipative cases, as we do in this paper.

In principle quantum dynamics can also be computed from the exact eigenstates, but this approach involves an exponentially large number of overlap integrals. Thus, results are often only applicable at long times [23]. Exact dynamical methods are restricted to small particle numbers [6], and there are similar limitations with matrix product state methods [5]. However, these methods make predictions that are qualitatively similar to those found here, even though for much smaller particle numbers; the details are treated elsewhere [24].

II. BOSE GAS HAMILTONIAN

The general Hamiltonian for a non-relativistic scalar Bose gas in three dimensions is

$$\hat{H}_{3D} = \hat{H}_0 + \hat{H}_I. \quad (2.1)$$

The quantum Bose field is $\hat{\Psi}(\mathbf{r})$ and the particle density is $\hat{n}(\mathbf{r}) = \hat{\Psi}^\dagger(\mathbf{r})\hat{\Psi}(\mathbf{r})$. The Hamiltonian is divided into a free-particle Hamiltonian \hat{H}_0 , with mass m and single-particle potential V :

$$\hat{H}_0 = \int \hat{\Psi}^\dagger H \hat{\Psi} d^3\mathbf{r}, \quad (2.2)$$

with $H = -\hbar^2\nabla^2/2m + V(\mathbf{r})$, and for parabolic trapping, $V(\mathbf{r}) = m\Sigma_i\omega_i^2 r_i^2/2$. There is a normally-ordered interaction term \hat{H}_I , with two-body interaction potential g :

$$\hat{H}_I = \frac{g}{2} \int \hat{\Psi}^\dagger \hat{\Psi}^\dagger \hat{\Psi} \hat{\Psi} d\mathbf{r}. \quad (2.3)$$

This Hamiltonian is number-conserving. As a result, the ground state or any energy eigenstate can always be chosen as a number eigenstate $|\Psi\rangle_N$, since \hat{N} and \hat{H} commute. For a dilute atomic BEC in the three-dimensional case has [25]:

$$g = \frac{4\pi\hbar^2 a}{m} \quad (2.4)$$

giving an approximate pseudo-potential where a is the S-wave scattering length. This must be combined with a momentum cutoff to eliminate corrections from renormalization.

A. One dimensional (1D) Bose gas

In one dimensional atomic waveguides the Bose gas is a quasi-condensate, usually generated from transverse confinement of an atomic Bose-Einstein condensate (BEC) [26]. If the bosons are confined to a single transverse mode, one obtains an 1D Bose gas theory, valid for low energies:

$$\begin{aligned} \hat{H}_{1D} &= \frac{\hbar^2}{2m} \int \hat{\Psi}_{1D}^\dagger H_1 \hat{\Psi}_{1D} dr_3 \\ &+ \frac{g_{1D}}{2} \int \left(\hat{\Psi}_{1D}^\dagger\right)^2 \hat{\Psi}_{1D}^2 dr_3, \end{aligned} \quad (2.5)$$

where, for an atomic Bose gas in a parabolic trap, $H_1 = -\hbar^2\partial_3^2/2m + m\omega_3^2 r_3^2/2$ and $g_{1D} = 2\hbar\omega_\perp a$, with an effective transverse trapping frequency of $\omega_\perp = \sqrt{\omega_1\omega_2}$.

In dielectric waveguide or fibre optical experiments [2, 27, 28], the mass and nonlinearity originates in the dispersion and nonlinearity of the waveguide. The effective

mass is given by $m_{\text{eff}} = \hbar/\omega''$, where ω'' is the second order dispersion. The nonlinearity is

$$g_{1D} = \frac{-3\hbar\omega'\chi^{(3)}\omega_0^2}{4\epsilon A c^2}, \quad (2.6)$$

where $\chi^{(3)}$ is the third order Bloembergen nonlinearity parameter in S. I. units, ω_0 is the laser carrier frequency, ω' is the group velocity, A is the effective mode cross-section, ϵ is the permittivity and c is the speed of light.

B. Dimensionless Hamiltonian

The one-dimensional Hamiltonian (2.5) has exact energy eigenstates in both the repulsive [29] and attractive [30] case. It can be transformed to dimensionless form on choosing a length scale r_0 and time scale t_0 such that $r_0^2 = \hbar t_0/2m$. Axial distance is scaled to give a dimensionless distance $z = r_3/r_0$, and similarly time is scaled to give $\tau = t/t_0$. The resulting Hamiltonian is written in the Lieb and Liniger [29] form, using a dimensionless wave-function $\hat{\psi} = \hat{\Psi}_{1D}\sqrt{r_0}$, as:

$$\hat{H} = \int dz \left[\hat{\psi}_{,z}^\dagger(z)\hat{\psi}_{,z}(z) + C \left(\hat{\psi}^\dagger(z)\right)^2 \hat{\psi}^2(z) \right]. \quad (2.7)$$

Here: $\hat{\psi}_{,z}(z) \equiv \partial_z \hat{\psi}(z) \equiv \partial \hat{\psi}(z)/\partial z$.

The following ‘Rosetta stone’ can be used to obtain dimensionless units for a trapped Bose-Einstein condensate [31, 32]:

$$\begin{aligned} \hat{H} &= \hat{H}_1/E_0 \\ E_0 &= \hbar/t_0 = \hbar^2/2mr_0^2 \\ C &= \frac{mg_{1D}r_0}{\hbar^2} = 2m\omega_\perp r_0 a/\hbar. \end{aligned} \quad (2.8)$$

One may also utilize mode operators for plane waves in a box of a dimensionless length:

$$\hat{\psi}(z) = \frac{1}{\sqrt{L}} \sum_k e^{ikz} \hat{a}_k = \frac{1}{\sqrt{2\pi}} \int dk e^{ikz} \hat{a}(k). \quad (2.9)$$

Since the dimensionless Lieb-Liniger parameter C depends on the length scale, for a uniform gas one can also define $\gamma = C/n_0$, where n_0 is the dimensionless density, to obtain a parameter that is independent of length scales. For solitons [33], one may simply defines r_0 as the characteristic initial soliton dimension, so that C is of the order of the inverse particle number N .

The resulting Heisenberg equation is the one-dimensional quantum nonlinear Schrödinger equation. An almost identical picture holds for 1D photonic systems [27, 33], except for Raman-Brillouin coupling to phonons [34, 35]. In either photonic and atomic experiments, there are additional dissipative couplings as well as linear and nonlinear losses and phase noise. These effects lead to additional terms in the equations, but here we focus on the simplest, non-dissipative case.

The particle density in momentum space is $\hat{n}_k = \hat{a}_k^\dagger \hat{a}_k$. Even with current BEC technology [36] there are typically at least Poissonian number fluctuations, which we include here for generality.

This equation and its extensions has been widely used to calculate quantum dynamical properties of Bose gases [33, 37] using phase-space techniques that originate in the work of Wigner [1] and Glauber [38], with quantitative experimental verification in photonic experiments [27, 39, 40].

III. EXACT QUANTUM DYNAMICS

The uniform, one-dimensional Bose gas with local interactions is exactly soluble. Thus, all the eigenfunctions and eigenvalues as well as the equilibrium density matrix can be written down. Yet there are exponentially many eigenfunctions, each rather complex. One would need to compute exponentially many multi-dimensional overlap integrals to exactly compute dynamics, even knowing these eigenstates. As a result, the exact solutions do not necessarily help one to make predictions about dynamical evolution from an arbitrary initial quantum state.

Surprisingly, therefore, exact solubility in this sense does not remove the barrier of exponential complexity. This prevents one from making general dynamical predictions. As a result, approximate methods are needed. However, as well as eigenvalues, this system has a large number of easily constructed conservation laws. These in turn, allow one to construct other dynamical variables. In this way one can make rigorous predictions about the time evolution which can be used to validate approximate methods.

A. Conservation laws

The usual three conserved operators that are considered are the conservation of particle number, momentum, and energy, arising from phase, space and time translational symmetry using Noether's theorem [17]. There is at least one further local symmetry in the case of the nonlinear Schrödinger equation in one dimension, which is termed \hat{H}_3 . While higher symmetries exist as well [7], these are not simple normally ordered local functions of quantum fields.

Using a standard notation [8, 41], one obtains locally conserved densities which are

$$\begin{aligned} \hat{h}_0 &= \hat{\psi}^\dagger(z)\hat{\psi}(z) \\ \hat{h}_1 &= \frac{i}{2} \left[\hat{\psi}_{,z}^\dagger(z)\hat{\psi}(z) - \text{h.c.} \right] \\ \hat{h}_2 &= \hat{\psi}_{,z}^\dagger(z)\hat{\psi}_{,z}(z) + C\hat{\psi}^{\dagger 2}(z)\hat{\psi}^2(z) \\ \hat{h}_3 &= \frac{i}{2} \left[\hat{\psi}_{,zz}^\dagger(z)\hat{\psi}_{,z}(z) + \frac{3C}{2} \left(\hat{\psi}^{\dagger 2}(z) \right)_{,z} \hat{\psi}^2(z) - \text{h.c.} \right]. \end{aligned} \quad (3.1)$$

The globally conserved quantities are then:

$$\hat{H}_j = \int_{-L/2}^{L/2} \hat{h}_j dz, \quad (3.2)$$

and one can make the identification with the usual Noether conserved quantities that $\hat{H}_0 = \hat{N}$, $\hat{H}_1 = \hat{P}$, $\hat{H}_2 = \hat{H}$.

These four conservation laws correspond to a locally conserved current [42], which means that they have local as well as global consequences. The consequences of these local charges and conservation laws have been widely discussed in recent literature relating to their applicability to generalized Gibbs ensembles [43, 44]. It is sometimes useful to write these as sums over mode operators. Define $\delta_{\mathbf{k}} = 1$ if $k_1 + k_2 = k_3 + k_4$ and $\delta_{\mathbf{k}} = 0$ otherwise, so that as well as the standard results of $\hat{N} = \sum_{\mathbf{k}} \hat{n}_{\mathbf{k}}$ and $\hat{P} = \sum_{\mathbf{k}} k \hat{n}_{\mathbf{k}}$, we obtain:

$$\begin{aligned} \hat{H} &= \sum_{\mathbf{k}} k^2 \hat{n}_{\mathbf{k}} + \frac{C}{L} \sum_{\mathbf{k}} \hat{a}_{k_1}^\dagger \hat{a}_{k_2}^\dagger \hat{a}_{k_3} \hat{a}_{k_4} \delta_{\mathbf{k}} \\ \hat{H}_3 &= \sum_{\mathbf{k}} k^3 \hat{n}_{\mathbf{k}} + \frac{3C}{2L} \sum_{\mathbf{k}} (k_1 + k_2) \hat{a}_{k_1}^\dagger \hat{a}_{k_2}^\dagger \hat{a}_{k_3} \hat{a}_{k_4} \delta_{\mathbf{k}}. \end{aligned} \quad (3.3)$$

These four conservation laws of the quantum nonlinear Schrödinger equation correspond to conservation laws of the classical nonlinear Schrödinger equation [45], although the higher order ones differ [46]. We will analyze these in the next two sections, where we show that these are also exactly conserved in the truncated Wigner approximation. To do this, one must take account of symmetrized operator ordering in these polynomial conservation laws, in order to make comparisons.

B. Exact dynamical laws

Since the operators \hat{H} are conserved, one can also use them to obtain exact dynamical solutions to time-varying quantities. This is always possible if the operator solutions can be expressed in terms of the conserved quantities. A useful example is the center-of-mass position spreading. This has an exact solution because the center-of-mass position only depends on the conserved total momentum. However, there are multiple possible definitions of this with a variable particle number, so one has to define the terminology. One issue is that a many-body system can have zero particles, and hence an undefined position.

In this paper we will use the quasi-intensive center of mass [20], which corresponds to measurements that are weighted by the instantaneous particle number, and normalized by the mean particle number, $\bar{N} = \langle \hat{N} \rangle$. This is nonsingular over the entire many-body Hilbert space, including particle numbers of zero. An alternative is to normalize by the number operator, but this has no well-defined inverse in general. Hence, we define the COM

position operator as:

$$\hat{z} = \frac{1}{\bar{N}} \int dz [z \hat{n}(z)]. \quad (3.4)$$

The commutator of \hat{z} with the total momentum $\hat{P} = \sum k \hat{n}_k$ can be calculated to give $[\hat{z}, \hat{P}] = i\hbar \hat{N}/\bar{N}$. Since \hat{z} commutes with interaction Hamiltonian \hat{H}_I , its time evolution is given by

$$\frac{d\hat{z}}{d\tau} = \frac{i}{\hbar} [\hat{H}, \hat{z}] = \frac{2\hat{P}}{\bar{N}}. \quad (3.5)$$

This is the usual first quantized expression, with an effective mass of $\bar{N}/2$. The center-of-mass position at time τ now has an exact solution in terms of the conserved momentum \hat{P} and the conserved particle number \hat{N} , for mass distributions localized in a region that does not overlap the boundaries at $\pm L/2$:

$$\hat{z}(\tau) = \hat{z}(0) + 2\hat{P}\tau/\bar{N}. \quad (3.6)$$

The above result allows one to calculate the mean variance $\Delta^2 z(\tau)$ in \hat{z} , which is:

$$\Delta^2 z(\tau) = \left\langle \left(\hat{z}(0) + 2\hat{P}\tau/\bar{N} \right)^2 \right\rangle - \bar{z}^2(\tau). \quad (3.7)$$

We now consider the initially stationary case where $\langle \hat{P} \rangle = \langle \hat{P} \hat{z}(0) \rangle = \langle \hat{z}(0) \hat{P} \rangle = 0$. Expanding the variance, one finds that:

$$\Delta^2 z(\tau) = \Delta^2 z(0) + \frac{4\tau^2}{\bar{N}^2} \langle \hat{P}^2 \rangle. \quad (3.8)$$

The position and momentum variance are not normally-ordered, and can also be re-expressed in normally ordered form as:

$$\begin{aligned} \hat{z}^2 &=: \hat{z}^2 : + \frac{1}{\bar{N}^2} \int dz (z^2 \hat{n}(z)) \\ \hat{P}^2 &=: \hat{P}^2 : + \sum k^2 \hat{n}_k. \end{aligned} \quad (3.9)$$

Here $: \dots :$ is used to indicate operator normal ordering. Since \hat{P} is conserved, this allows the calculation of the center-of-mass variance purely in terms of the *initial* operator expectation values.

C. Poissonian example

Current experiments in photonic or Bose condensate systems usually have at least a Poissonian variance of particle numbers, with mean \bar{N} and number variance \bar{N} . The density matrix for a Poissonian probability distribution of particle number states is equivalent to a phase mixture of coherent states $|\alpha(z) e^{i\theta}\rangle$, with a coherent amplitude $\alpha(z) e^{i\theta}$. That is:

$$\hat{\rho} = \frac{1}{2\pi} \int d\theta |\alpha(z) e^{i\theta}\rangle \langle \alpha(z) e^{i\theta}|. \quad (3.10)$$

Thus, for the case $\theta = 0$, one has $\hat{\psi}(z) |\alpha(z)\rangle = \alpha(z) |\alpha(z)\rangle$, and $\hat{a}_k |\alpha(z)\rangle = \alpha_k |\alpha(z)\rangle$. Since none of the quantities calculated here are phase-sensitive, we let $\theta = 0$ and calculate results without having to number or phase-average, by using an initial density matrix that corresponds to a coherent state, following methods pioneered by Glauber [38, 47] in quantum optics, so that $\hat{\rho}^{\text{eff}} = |\alpha(z)\rangle \langle \alpha(z)|$.

The true density matrix is a mixed state, but this is equivalent to $\hat{\rho}^{\text{eff}}$ for phase-insensitive observables. It is useful to define number densities, $n^C(z) = |\alpha(z)|^2$, and mode occupations $n_k^C = |\alpha_k|^2$. In this case, one can readily calculate any normally ordered quantity, so that:

$$\langle \hat{N} \rangle = \sum n_k^C = \int dz n^C(z) \quad (3.11)$$

$$\langle \hat{P} \rangle = \sum k n_k^C = \frac{i}{2} \int dz [\alpha(z) \partial_z \alpha^*(z) - \text{h.c.}]$$

$$\langle \hat{H} \rangle = \sum k^2 n_k^C + C \int dz (n^C(z))^2$$

$$\langle \hat{H}_3 \rangle = \sum k^3 n_k^C + \frac{3iC}{4} \int dz [(\alpha^{*2}(z))_{,z} \alpha^2(z) - \text{h.c.}].$$

This implies that both position and momentum variance measurements can be calculated using their normally-ordered expressions given in Eq. (3.9), together with the coherent state eigenvalue relations, as

$$\langle \Delta \hat{z}^2 \rangle = \frac{1}{\bar{N}^2} \int dz (z^2 n^C(z))$$

$$\langle \Delta \hat{P}^2 \rangle = \sum k^2 n_k^C. \quad (3.12)$$

Physically such an initial state would correspond to a mixture of ground states of a non-interacting BEC with an appropriate potential and Poissonian particle number, or the output of a stabilized coherent pulsed laser.

D. Gaussian and hyperbolic secant cases

As typical examples, we now take the common cases of an initial gaussian or hyperbolic secant pulse shape.

Gaussian case In the case of an initial gaussian average number density with $n^C(z) = \bar{N} \exp(-z^2/\sigma^2)/\sqrt{\pi\sigma^2}$, one has $\langle \hat{N} \rangle = \bar{N}$, $\langle \hat{P} \rangle = \langle \hat{H}_3 \rangle = 0$, and the analytic result is that:

$$\langle \hat{H} \rangle = \frac{\bar{N}}{2\sigma^2} + \frac{C\bar{N}^2}{\sigma\sqrt{2\pi}}$$

$$\langle \Delta \hat{P}^2 \rangle = \frac{\bar{N}}{2\sigma^2}$$

$$\langle \Delta \hat{z}^2(\tau) \rangle = \frac{1}{\bar{N}} \left[\frac{\sigma^2}{2} + \frac{2\tau^2}{\sigma^2} \right]. \quad (3.13)$$

Hyperbolic secant case In the case of an initial hyperbolic secant average number density with $n^C(z) = \bar{N} \text{sech}^2(z/\sigma) / (2\sigma)$, one has the analytic result that:

$$\langle \hat{H} \rangle = \frac{\bar{N}}{3\sigma^2} + \frac{C\bar{N}^2}{3\sigma} \quad (3.14)$$

$$\langle \Delta \hat{P}^2 \rangle = \frac{\bar{N}}{3\sigma^2}$$

$$\langle \Delta \hat{z}^2(\tau) \rangle = \frac{1}{\bar{N}} \left[\frac{\pi^2 \sigma^2}{12} + \frac{4\tau^2}{3\sigma^2} \right]. \quad (3.15)$$

These predictions hold for an interacting as well as a free field. They are true for any strength or sign of interaction. As such, they provide a means to test theoretical approximations to interacting many-body systems in one dimension. The test was used recently to test multi-configurational variational many-body approximations [4]. This analysis showed that the number of natural modes needed for correct results was much higher than previously thought. Accordingly, it is a useful test of other many-body approximations as well.

IV. TRUNCATED WIGNER CONSERVATION LAWS

The nonlinear Schrödinger equation is the lowest order term in an expansion of the Wigner phase-space representation [1] equation of motion in powers of $1/N$. When combined with stochastic initial conditions which replicate the initial state, this is called the truncated Wigner (TW) approximation. It is known to give quantitatively correct predictions for one-dimensional quantum squeezing dynamics when compared to exact positive-P representation methods [2, 48]. This approach has also been verified experimentally to high accuracy [28, 40, 49]. It can be extended to treat linear and nonlinear dissipation channels [50]. As result, it is important to understand how accurate this approximation is.

Moments of a Wigner distribution correspond to symmetrized rather than normally ordered quantum observables. Symmetrization is treated in the Appendix, where we show that the normal-ordered quantum conservation laws are equal to sums over symmetrized conservation laws. Since the symmetrized forms of these operators can diverge at large momentum cutoff, it is essential to include a momentum cutoff in the calculations. This is included in all the momentum sums below.

To make it simpler to compare results with different operator orderings, we will use the notation $\langle \hat{O} \rangle_W$ to indicate a quantum observable evaluated using the truncated Wigner method. One would have exact equality without truncation, but after truncation there are time-dependent errors that scale as a power of $1/N$, depending on the observable.

We will show that all four conservation laws are exact in both the full quantum dynamics and in the truncated Wigner approach. This provides further evidence for the

accuracy of the method, for one-dimensional problems. This result is due to the fact that the classical nonlinear Schrödinger equation also has an infinite number of classical conservation laws [51]. Therefore we simply have to show that for the first four conservation laws, the differences between the exact conserved quantities and the symmetrized observables equivalent to the classical conservation laws are also conserved quantities.

A. Wigner representation

The Wigner distribution $W[\psi]$ is a representation of any state of a quantum field [1]. It generally is not positive definite. The time-evolution equation for the density matrix can be transformed [52] into a differential equation for $W[\psi]$. This has third or higher order derivatives if the Hamiltonian is nonlinear, which can be truncated [2, 50, 53], to give a second-order Fokker-Planck equation. The truncated terms are the highest order terms in a $1/N$ expansion for N particles.

To obtain numerical results, and to reduce sampling errors from vacuum fluctuations, a momentum cutoff $k_c = 2\pi/\Delta z$ is introduced. When there is a momentum cutoff in an M -mode quantum field calculation there are no more than M independent dynamical variables. As a result, for a finite momentum cutoff, we assume the independent field operators $\hat{\psi}(z_j)$ comprise a discrete lattice of M points z_j , with a spacing of $\Delta z = L/M$ in position space and of M points k_j , with spacing $\Delta k = k_c/M$ in momentum space [27, 33], each symmetrically distributed about zero such that:

$$\hat{\psi}(z_j) = \frac{1}{\sqrt{M\Delta z}} \sum_k e^{ikz_j} a_k. \quad (4.1)$$

Hereinafter the summation over k means the summation over discrete values $k_l = -k_c/2 + \Delta k/2 + l\Delta k$, $l = 0 \dots M-1$ for even M and $k_l = -k_c/2 + l\Delta k$ for odd M .

The fundamental commutator for field operators is a tempered or smoothed commutator,

$$\tilde{\delta}(z-y) = [\hat{\psi}(z), \hat{\psi}^\dagger(y)] = \frac{1}{L} \sum_k e^{ik(z-y)}. \quad (4.2)$$

Hence the commutator of two Bose fields at the same lattice point is not infinite:

$$[\hat{\psi}, \hat{\psi}^\dagger] = \frac{1}{L} \sum_k [\hat{a}_k, \hat{a}_k^\dagger] = \frac{1}{\Delta z}, \quad (4.3)$$

The result is an equivalent partial differential equation for the equivalent Wigner field ψ [2, 9, 50]:

$$\frac{d\psi}{dt} = i\nabla^2\psi - 2iC\psi(|\psi|^2 - 1/\Delta z). \quad (4.4)$$

Here the Laplacian differential operator is defined on a lattice either through finite differences or spectral transform methods, and quantum noise comes from random initial conditions. Although the conservation laws do not depend on the initial conditions, we treat a Poissonian number distribution in the numerical examples. This is equivalent to a coherent state (see Section III C), with $\hat{\rho}(t=0) = |\alpha(z)\rangle\langle\alpha(z)|$, and $|\alpha(z)|^2 = n(z)$. In the Wigner representation this initial state corresponds to a complex Gaussian probability. After sampling, the initial Wigner fields for a coherent state with constant phase are then:

$$\psi(z) = \alpha(z) + \frac{1}{\sqrt{2}} \sum_k \frac{1}{\sqrt{L}} \eta_k e^{ikz}, \quad (4.5)$$

where η_k are complex random numbers correlated as $\langle\eta_k \eta_{k'}^*\rangle = \delta_{kk'}$, $\langle\eta_k \eta_{k'}\rangle = 0$. The average over the distribution is performed by generating N_s multiple random initial states. Finally, one averages over the N_s independent field modes with equal probability, after evolving them in time.

The Wigner representation gives a direct representation of symmetrically ordered operators. Normally-ordered observables require the transformation of a Wigner average from a symmetrically ordered to a normally ordered form, using the techniques of the previous section. This also removes the divergence of symmetrically-ordered observables at large momentum cutoff.

The expectation values of symmetrically ordered operator expressions can be obtained approximately by integrating this equation over multiple independent trajectories to produce a set of values $\psi^{(j)}$ and averaging over a corresponding function of these values, where the truncation error depends on the evaluated operator [54, 55] and the particle number:

$$\langle\langle\hat{O}(\hat{\psi}, \hat{\psi}^\dagger)\rangle\rangle \approx \langle\langle\hat{O}\rangle\rangle_W = \langle O \rangle_W. \quad (4.6)$$

Here $\{\dots\}$ indicates symmetrization, so the last average refers to the numerically evaluated, sampled average of the classical function $O(\psi, \psi^*)$, which is approximately equal to the symmetrically ordered quantum expectation value:

$$\langle O \rangle_W \equiv \lim_{N_s \rightarrow \infty} \frac{1}{N_s} \sum_j O(\psi^{(j)}, (\psi^{(j)})^*). \quad (4.7)$$

where N_s is the number of stochastic trajectories.

More generally, $\langle\hat{O}\rangle_W$ will be used to refer to *any* quantum observable evaluated using this technique, with appropriate commutator terms added to transform the operator function into a symmetrically ordered function, as described in the Appendix.

B. Conservation laws as Wigner averages

Since using symmetrization will involve sums over momenta, it is convenient to define these sums in a uniform way as

$$M_n = \frac{1}{\Delta k^n} \sum_k k^n. \quad (4.8)$$

Obviously, $M_0 = M$ and $M_n = 0$ for odd n ; one can find $M_2 = M(M^2 - 1)/12$ (see Appendix for details). Applying symmetrization to all four conservation laws gives, as shown in the Appendix, the following relationship between the operators:

$$\begin{aligned} \hat{N} &= \left\{ \hat{N} \right\} - \frac{1}{2} M \\ \hat{P} &= \left\{ \hat{P} \right\} \\ \hat{H} &= \left\{ \hat{H} - \frac{2C}{\Delta z} \hat{N} \right\} - \frac{1}{2} M_2 \Delta k^2 + \frac{MC}{2\Delta z} \\ \hat{H}_3 &= \left\{ \hat{H}_3 - \frac{3C(M+1)}{L} \hat{P} \right\}. \end{aligned} \quad (4.9)$$

Here, Δz is the cell size used for the momentum cutoff, as defined in (4.1). Since the truncated Wigner method follows the dynamics of the nonlinear Schrödinger equation [51], it conserves the following classical quantities:

$$N = \int dz [\psi^*(z)\psi(z)] \quad (4.10)$$

$$P = \frac{i}{2} \int dz [\psi_{,z}^*(z)\psi(z) - \psi^*(z)\psi_{,z}(z)]$$

$$H = \int dz [\psi_{,z}^*(z)\psi_{,z}(z) + C\psi^{*2}(z)\psi^2(z)]$$

$$H_3 = \frac{i}{2} \int dz \left[\psi_{,zz}^*(z)\psi_{,z}(z) - \frac{3C}{2}\psi^{*2}(z)(\psi^2(z))_{,z} - \text{c.c.} \right].$$

We note the following relationships, due to symmetric ordering:

$$\langle H_n \rangle_W = \left\langle \left\{ \hat{H}_n \right\} \right\rangle. \quad (4.11)$$

Evaluating the quantum operator expectation values in the Wigner representation, then gives, for the case of a symmetric momentum sum:

$$\begin{aligned} \langle \hat{N} \rangle_W &= \langle N \rangle_W - \frac{1}{2} M \\ \langle \hat{P} \rangle_W &= \langle P \rangle_W \\ \langle \hat{H} \rangle_W &= \left\langle H - \frac{2C}{\Delta z} N \right\rangle_W - \frac{1}{2} M_2 \Delta k^2 + \frac{MC}{2\Delta z} \\ \langle \hat{H}_3 \rangle_W &= \left\langle H_3 - \frac{3C(M+1)}{L} P \right\rangle_W. \end{aligned} \quad (4.12)$$

In each case the correction terms that are obtained are either constants or conserved quantities. This means that all four quantum conservation laws are equally conserved in both the truncated Wigner approximation, and in the exact operator equations.

C. COM dynamical results

Since the classical moments \mathbf{H} are conserved, one can also use them to obtain exact dynamical solutions to certain time-varying quantities in the truncated Wigner method. But will these be the same as the quantum results? As before, a useful case is the center-of-mass position. Hence, we can define:

$$\bar{z} = \frac{1}{\bar{N}} \int dz [zn(z)]. \quad (4.13)$$

The center-of-mass position \bar{z} at time τ has an exact solution of $\bar{z}(\tau) = \bar{z}(0) + 2P\tau/\bar{N}$ for each truncated Wigner trajectory, in terms of the classically conserved momentum P and the number N , given a distribution localized in a region that does not overlap the boundaries at $\pm L/2$. In the case of a stochastic initial condition, this allows one to calculate the mean Wigner position variance $\Delta_{Wz}^2(\tau)$. We consider the symmetric pulse case where $\langle \bar{z}(0) \rangle_W = \langle P \rangle_W = \langle \bar{z}(0)P \rangle_W = 0$. Thus:

$$\Delta_{Wz}^2(\tau) = \langle \bar{z}^2(\tau) \rangle_W - \langle \bar{z}(\tau) \rangle_W^2 = \langle \bar{z}^2(\tau) \rangle_W. \quad (4.14)$$

Next we assume that we can approximately write the field as $\psi = \psi_C + \psi_V$, with a coherent, localized part ψ_C and a stochastic, delocalized background part, ψ_V . The delocalized stochastic vacuum is time-invariant, that is, it experiences no COM spreading. This is consistent with the results given above, since the stochastic terms are delocalized, and therefore have boundary terms that cancel the COM spreading. Expanding this, one finds that, within the truncated Wigner approximation:

$$\langle \bar{z}^2(\tau) \rangle_W = \langle \bar{z}^2(0) \rangle_W + \frac{4\tau^2}{\bar{N}^2} [\langle P^2 \rangle_W - \langle P^2 \rangle_B], \quad (4.15)$$

Here $\langle P^2 \rangle_B$ is a boundary correction which is caused by the delocalized nature of the stochastic vacuum. From the symmetrization results in the Appendix, the quantum momentum variance is given by $\langle \hat{P}^2 \rangle_W = \langle P^2 \rangle_W - M_2\Delta k^2/4$. Since there can be no COM spreading in a pure stochastic vacuum with $\langle \hat{P}^2 \rangle_W = 0$, we can estimate the boundary correction as $\langle P^2 \rangle_B \approx M_2\Delta k^2/4$. This is exact for a linear Hamiltonian, where the two terms do not interact, but is generally approximate, not exact.

From the symmetrization results in the Appendix, the quantum operator averages can be calculated from the

Wigner classical averages using commutation relations, giving:

$$\langle \hat{z}^2(\tau) \rangle_W = \langle \bar{z}^2(\tau) \rangle_W - \frac{M_2\Delta z^2}{4\bar{N}^2} \quad (4.16)$$

Combining these expressions, the truncated Wigner result is approximately equal to the known quantum result. However, we expect that this boundary subtraction is not exact. We find numerically that there is a small correction that scales as $1/\bar{N}^{3/2}$:

$$\langle \hat{z}^2(\tau) \rangle_W \approx \langle \bar{z}^2(0) \rangle_W + \frac{4\tau^2}{\bar{N}^2} \langle \hat{P}^2 \rangle_W + O(\bar{N}^{-3/2}) \quad (4.17)$$

Since P is conserved, this allows the calculation of the center-of-mass variance from the *initial* stochastic expectation values. Now, since the initial Wigner distribution can be chosen to correspond exactly to a quantum many-body state, it is straightforward to use the symmetrization rules to obtain the correct operator results initially. Yet while the classical dynamical solutions in the truncated Wigner method look superficially like the full quantum solutions, they are not the same.

In summary, compared to the exact quantum prediction of Eq. (3.8), we see that evaluating the COM variance with the truncated Wigner method gives rise to an error of approximate order $\bar{N}^{-3/2}$ relative to the exact result. This is caused by the fact that the vacuum fluctuations behave as real physical fields when truncation is employed in the presence of nonlinearity, so that the boundary correction is no longer exact. This error, however, is small for large \bar{N} , as we show later in the numerical results.

V. NUMERICAL RESULTS

We illustrate these analytical results with numerical calculations for higher order soliton or ‘breather’ fragmentation in an attractive 1D Bose gas. The breather oscillates with the period $\tau_b = \pi/4$ [56], and Figs. 1, 2 and 3 show the density profiles for $N = 10^3$, 3×10^3 and 10^4 at separate oscillations of the breather at the minima and the maxima of the central density. Classically, all the oscillations would be identical to the first.

This quantum many-body dynamical problem has been the topic of several publications. The first [3] used an MCTDHB approach with $N = 1000$ and two spatial modes. This calculation was recently criticized as being not fully converged [4]. The evidence was that the numerical predictions were in violation of known exact quantum COM expansion results. Other known results use methods that are more reliable, but are restricted to small particle numbers [5, 6].

Here we use the truncated Wigner method, which is a $1/N$ expansion, as explained above. This allows large particle numbers, that is, $N \geq 1000$, and large numbers of independent modes. Numerical data was calculated

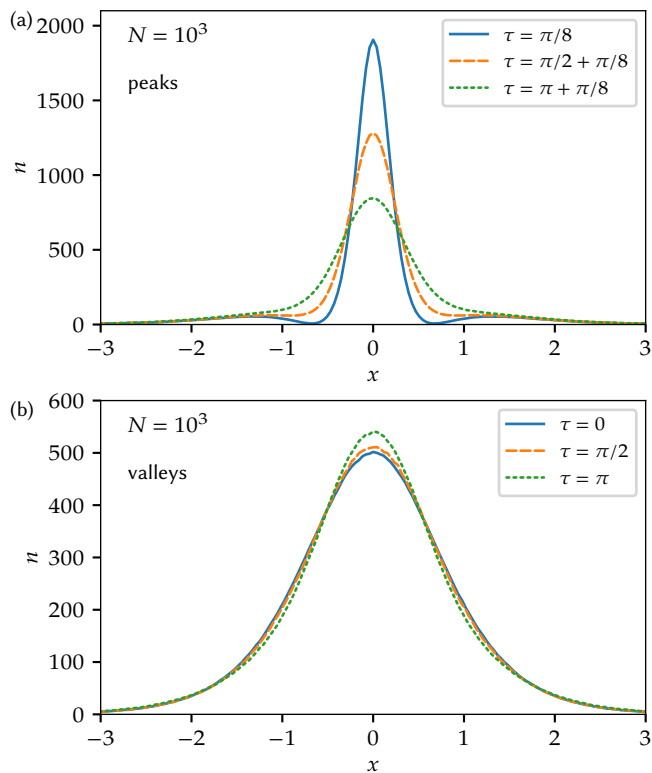


Figure 1. Density profiles of a breather in the peaks (a) and valleys (b) of the zeroth, second and fourth oscillations. The simulation has $N = 10^3$, $C = -8/N$, $M = 512$, $L = 20$, 10^5 trajectories, 10^5 time steps.

with two independent public domain numerical codes [57, 58], using a fourth-order Runge-Kutta interaction picture algorithm [59], and periodic boundary conditions. All four known local conservation laws are satisfied within random sampling errors. Exact COM spreading results are recovered to a very good approximation, except for a systematic error of order $N^{-3/2}$, which is negligible compared to other effects.

A. Simulation Parameters

We consider a prototypical quantum experiment where an initial state is evolved in time. The initial quantum state considered is a Poissonian mixture of uncorrelated particles with mean value $\bar{N} = 10^2 - 10^4$.

The initial condition corresponds to the classical soliton shape that would occur with some small initial coupling of $C_i = -2/N$. This is chosen to correspond to previous MCTDHB calculations [3, 4], for purposes of comparison. With r_0 as the initial size, one finds in dimensionless units,

$$\alpha(z) = \sqrt{N/2} \operatorname{sech}(z). \quad (5.1)$$

This Poissonian initial state is chosen as being typical of experiments, which use a mixture of initial bo-

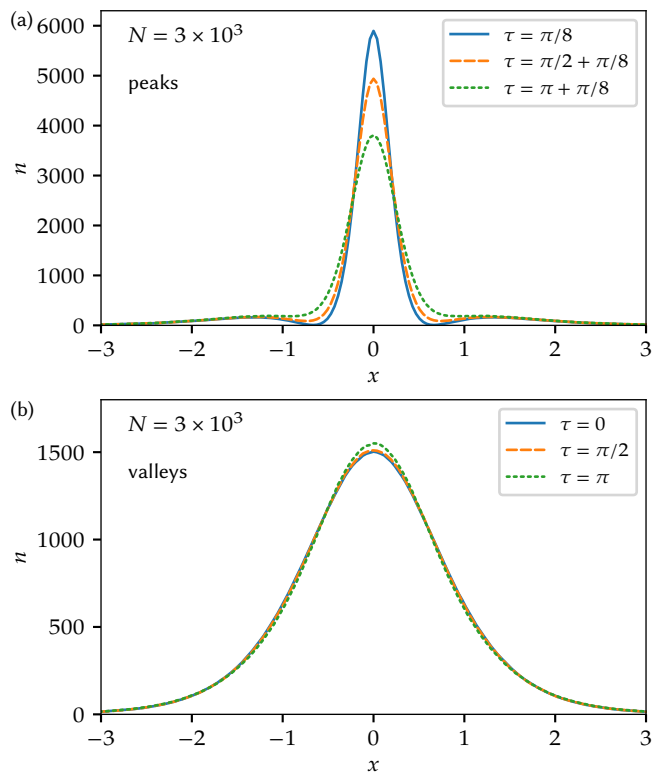


Figure 2. Density profiles of a breather in the peaks (a) and valleys (b) of the zeroth, second and fourth oscillations. The simulation has $N = 3 \times 10^3$, $C = -8/N$, other parameters are the same as in Fig. 1.

son numbers [36]. Thus, the initial boson number is $N = \bar{N} \pm \sqrt{\bar{N}}$, where $\bar{N} = 10^2 - 10^4$. The standard deviation is $\pm 1 - 10\%$, which is of the order of measured number fluctuations for this type of ultra-cold atomic physics experiment.

B. Conservation laws

We focus here on the question of the actual numerical values of conservation laws. The earlier calculations demonstrate clearly that these are all conserved, even after including the corrections due to symmetrization. However, it is also interesting to investigate how accurately they are conserved, given the inevitable sampling error in this method.

The first results we plot are the first four integrals N , P , H and H_3 , that are conserved during the evolution. To take into account the expected scaling of the results with simulation parameters, we normalize N and H by \bar{N} . The momentum-dependent quantities are zero on average, as expected, but their fluctuations are strongly dependent on the momentum cutoff. Accordingly, we normalize P by $1/\Delta z$, and H_3 by $1/\Delta z^3$. Fig. 4 shows that all four conservation laws are within a one standard deviation sampling error of their exact values at all

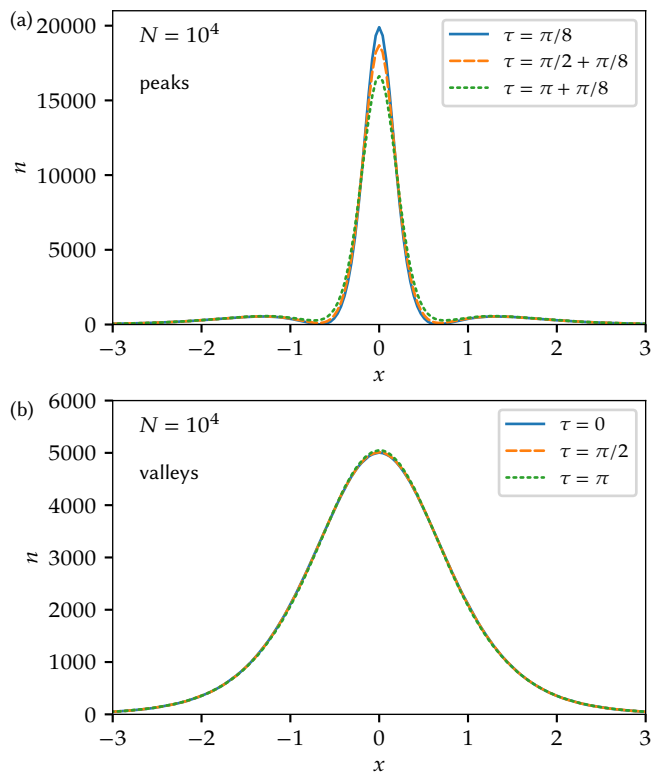


Figure 3. Density profiles of a breather in the peaks (a) and valleys (b) of the zeroth, second and fourth oscillations. The simulation has $N = 10^4$, $C = -8/N$, other parameters are the same as in Fig. 1.

times: $\langle N \rangle / \bar{N} = 1$, $\langle H \rangle / \bar{N} = (1 + C\bar{N}) / 3$ (as given by Eq. (3.14)), $\langle P \rangle = \langle H_3 \rangle = 0$.

C. Center-of mass spreading

To test a quantity that changes over time, we plot a calculation of center of mass uncertainties, compared with exact results. In Fig. 5, we show the center-of-mass position uncertainty predicted in our numerical calculations.

These results are in excellent agreement with exact results, apart from sampling error and a small boundary-related error. In Fig. 6, the residual error is plotted as a function of \bar{N} .

This shows that this residual error is an effect that scales as $1/\bar{N}^{3/2}$, which is expected from early sections, together with the fundamental result that the TW method is a truncated $1/\bar{N}$ expansion. The COM variance itself is predicted to scale as $1/\bar{N}$, so that the relative error is of order $1/\sqrt{\bar{N}}$, and becomes extremely small even in relative terms when \bar{N} is increased.

This is in strong contrast with MCDTHB variational methods. In this method, the number of modes available for use is strongly restricted by exponential complexity issues. The number is typically 2–3 in published results. The resulting calculations give COM variance predictions

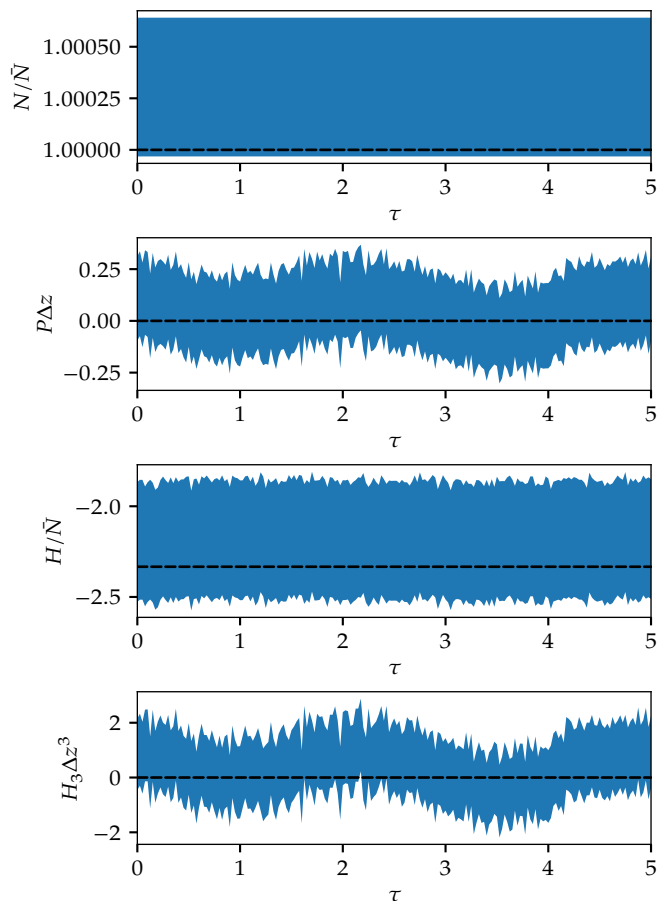


Figure 4. First four integrals in the simulation with $N = 10^3$, $C = -8 \times 10^{-3}$, $M = 512$, $L = 20$, 10^5 trajectories, 10^5 time steps. The blue band corresponds to the sampling error, the black dashed line shows the expected value.

that oscillate in time, and can either be much greater or smaller, even by orders of magnitude, than the exact results [4].

The sampling errors can be reduced here simply by taking more samples, and are smaller than expected experimental uncertainties in such measurements. Truncated Wigner methods are not immune to truncation error [60, 61]. However, the agreement with these exact tests is excellent, especially at large N , showing that for this type of experiment one might expect reliable results for other measurements. We see that with a large number of computed trajectories to reduce sampling error, the numerical conservation law results are indistinguishable from the exactly known behavior, for $N \geq 1000$.

VI. CONCLUSION

We have shown that the truncated Wigner approximation conserves all four local conservation laws of the one-dimensional quantum nonlinear Schrödinger equation. It also agrees to very high accuracy with the known exact

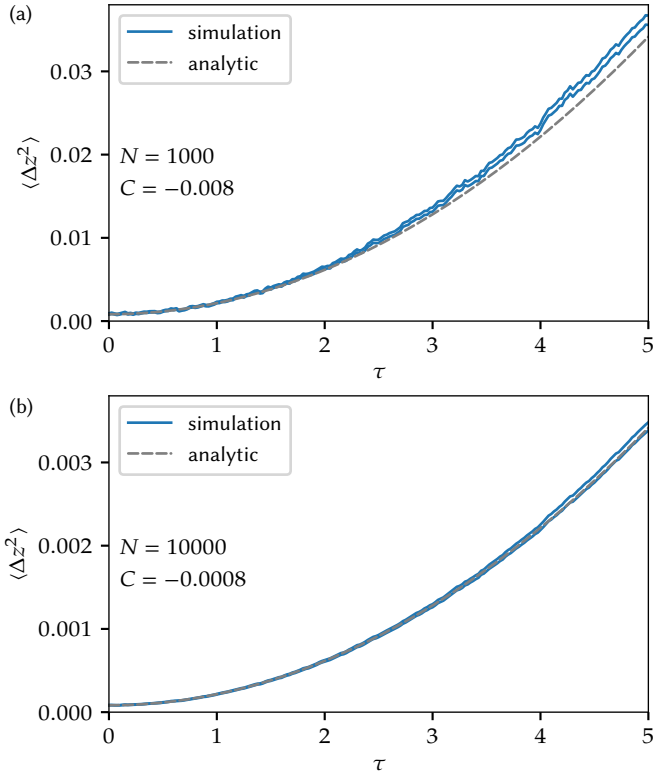


Figure 5. Position uncertainty $\langle \Delta z^2 \rangle$ over time as compared with the analytical prediction. Simulation with $N = 10^3$, $C = -8 \times 10^{-3}$ (a) and $N = 10^4$, $C = -8 \times 10^{-4}$ (b), $M = 512$, $L = 20$, 10^5 trajectories, 10^5 time steps. The area between the simulation curves (solid blue lines) denotes the estimated sampling error. The dashed grey line corresponds to the analytical expression (4.16). The small discrepancy between the predicted and sampled results at $N = 1000$ is explained in the text.

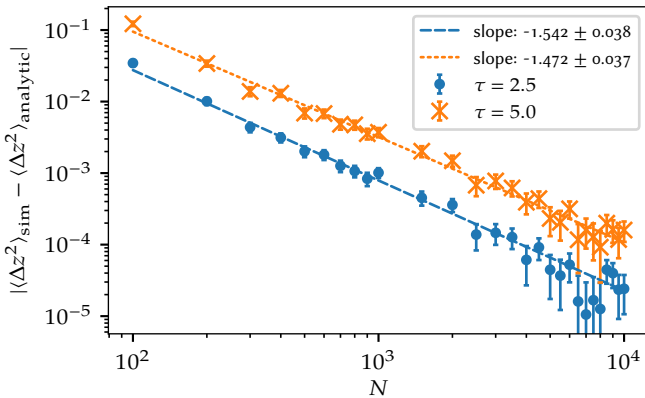


Figure 6. Errors in the position uncertainty $\langle \Delta z^2 \rangle$ as a function of N , at $\tau = 2.5$ and $\tau = 5$. Simulations have $N = 10^2 - 10^4$, $C = -8/N$. Other parameters as in Fig. 5. The error bars denote the estimated sampling error.

results for center-of-mass spreading, except for small corrections of order $N^{-3/2}$ for N particle simulations.

The conservation law and COM agreement obtained with the TW method may help to explain why this method was previously successful in agreeing both with exact quantum stochastic methods and experimental tests for photonic soliton quantum squeezing and entanglement [62].

In essence, quantum dynamical behaviour is restricted by conservation laws, and a technique that preserves these exactly has greatly reduced errors as a result. The present numerical and analytical results support numerical truncated Wigner predictions of a gradual quantum fragmentation of higher-order soliton breathers that appears elsewhere [24], in regimes that should be readily testable in BEC experiments.

ACKNOWLEDGMENTS

We would like to acknowledge helpful discussions with J. Brand and J. Cosme. This work was performed in part at Aspen Center for Physics, which is supported by National Science Foundation grant PHY-1607611.

APPENDIX: SYMMETRIZATION

The symmetrization results calculated here are exact, and simply follow as a result of the operator commutation relations. They are needed in order to relate normally ordered conservation laws to the ones calculated in the Wigner representation. We show in the main text that the significance of this result is that all four laws are conserved by truncated Wigner dynamics, in which the time evolution is a classical field evolution from a statistical mixture that corresponds to quantum fluctuations.

We start with some general results on symmetrization, then use these results to obtain exact results for conservation laws in symmetrized form. The symmetrization relations for the single-mode number operator is:

$$\{\hat{n}\} = \frac{1}{2} [\hat{a}^\dagger \hat{a} + \hat{a} \hat{a}^\dagger] = \hat{n} + \frac{1}{2}, \quad (6.1)$$

and for the mode number operator squared,

$$\{\hat{n}^2\} = \frac{1}{6} [\hat{a}^{\dagger 2} \hat{a}^2 + \hat{a}^\dagger \hat{a} \hat{a}^\dagger \hat{a} + \hat{a}^\dagger \hat{a}^2 \hat{a}^\dagger + \hat{a} \hat{a}^{\dagger 2} \hat{a} + \hat{a} \hat{a}^\dagger \hat{a} \hat{a}^\dagger + \hat{a}^2 \hat{a}^{\dagger 2}], \quad (6.2)$$

which simplifies to the form:

$$:\hat{n}^2: = \{\hat{n}^2\} - 2\{\hat{n}\} + \frac{1}{2}. \quad (6.3)$$

Another useful result is that:

$$\hat{n}^2 = \{\hat{n}^2\} - \{\hat{n}\}. \quad (6.4)$$

Lattice and momentum sums

As described in the main text, with a momentum cutoff the commutator of two Bose fields at the same point is finite:

$$\left[\hat{\psi}, \hat{\psi}^\dagger\right] = \frac{1}{L} \sum_k \left[\hat{a}_k, \hat{a}_k^\dagger\right] = \frac{1}{\Delta z}, \quad (6.5)$$

and therefore the symmetrization relation for the number density is:

$$\hat{n}(z) = \{\hat{n}(z)\} - \frac{1}{2\Delta z}. \quad (6.6)$$

Similarly, one obtains, for the square of the number density:

$$:\hat{n}^2(z): = \{\hat{n}^2(z)\} - \frac{2}{\Delta z} \{\hat{n}(z)\} + \frac{1}{2\Delta z^2}. \quad (6.7)$$

When using a finite momentum cutoff, one must replace the integration in the Hamiltonian with sums over the independent fields, giving $\int dz \rightarrow \sum_z \Delta z$. As introduced in the main text we define sums over integer powers occurring in mode sums as:

$$M_n = \frac{1}{\Delta k^n} \sum_k k^n$$

Remembering that the summation over k means the summation over discrete values $k_l = -k_c/2 + \Delta k/2 + l\Delta k$, $l = 0 \dots M-1$ for even M and $k_l = -k_c/2 + l\Delta k$ for odd M , we get

$$M_n = \begin{cases} \sum_{j=(1-M)/2}^{(M-1)/2} j^n & (\text{odd } M) \\ 2 \sum_{j=1}^{M/2} (j-1/2)^n & (\text{even } M). \end{cases}$$

For M modes, we have $M_0 = M$, $M_1 = 0$ and

$$M_2 = M(M^2 - 1)/12. \quad (6.8)$$

Number and momentum symmetrization

The normally ordered total number operator is $\hat{N} = \sum_k \hat{n}_k$. Using the result that $\hat{n}_k = \{\hat{n}_k\} - 1/2$, one immediately obtains:

$$\hat{N} = \left\{ \hat{N} \right\} - \frac{M}{2}. \quad (6.9)$$

This shows that the symmetrized number operator is also a conserved quantity, as it only differs from the conserved number operator by a constant. The fact that the constant is infinite in the limit of large momentum cutoff is immaterial, as quantum field theories in general always require finite momentum cutoffs in order have a reasonable physical interpretation.

The normally ordered total momentum operator is $\hat{P} = \sum_k k \hat{n}_k$. Using the result that $\hat{n}_k = \{\hat{n}_k\} - 1/2$, one uses the odd symmetry of the momentum sum to obtain $M_1 = 0$, to give:

$$\hat{P} = \left\{ \hat{P} \right\}.$$

Energy symmetrization

The normally ordered energy operator is best written as:

$$\hat{H} = \sum_k k^2 \hat{n}_k + C \int dz \hat{\psi}^{\dagger 2}(z) \hat{\psi}^2(z). \quad (6.10)$$

This is divided up into a kinetic and potential energy part, $\hat{H} = \hat{H}^K + \hat{H}^P$. The first part is similar to the number conservation expression, so that one obtains:

$$\hat{H}^K = \left\{ \hat{H}^K \right\} - \Delta k^2 \frac{M_2}{2}. \quad (6.11)$$

The remaining term is:

$$\hat{H}^P = C \int dz \hat{\psi}^{\dagger 2}(z) \hat{\psi}^2(z), \quad (6.12)$$

which is easily symmetrized in position space, by using the general results given above, to obtain:

$$\hat{H}_2 = \left\{ \hat{H}_2 \right\} - \frac{2C}{\Delta z} \left\{ \hat{H}_0 \right\} - \Delta k^2 \frac{M_2}{2} + \frac{MC}{2\Delta z}. \quad (6.13)$$

H_3 symmetrization

The normally ordered \hat{H}_3 operator is divided up into a kinetic and potential energy term, $\hat{H}_3 = \hat{H}_3^K + \hat{H}_3^P$, which are best treated in momentum space, using (3.3). The first term is unchanged by the symmetrization, as it is an odd momentum sum, hence $\hat{H}_3^K = \left\{ \hat{H}_3^K \right\}$.

The second term can be treated in two parts. Owing to the delta function in the summation, if $k_1 = k_3$ then $k_2 = k_4$, and vice-versa. Hence, if $k_1 \neq k_3$ and $k_1 \neq k_4$, then $k_2 \neq k_3$ and $k_2 \neq k_4$. We call this part (A). If $k_1 = k_3 \neq k_4$, then $k_2 = k_4 \neq k_1$. There are two permutations of this type, which comprise part (B), and finally if $k_1 = k_2 = k_3 = k_4$, one has part (C). Thus, $\hat{H}_3^P = \hat{H}_3^A + \hat{H}_3^B + \hat{H}_3^C$ where:

$$\begin{aligned} \hat{H}_3^B &= \frac{3C}{L} \sum_{k_1 \neq k_2} (k_1 + k_2) \hat{n}_{k_1} \hat{n}_{k_2} \\ &= \frac{3C}{L} \sum_{k_1 \neq k_2} (k_1 + k_2) \{ \hat{n}_{k_1} \hat{n}_{k_2} - \hat{n}_{k_1} \}, \end{aligned} \quad (6.14)$$

and similarly, using the symmetrization rules

$$\begin{aligned}\hat{H}_3^C &= \frac{3C}{2L} \sum_k 2k : \hat{n}_k^2 : \\ &= \frac{3C}{2L} \sum_k 2k \{ \hat{n}_k^2 - 2\hat{n}_k \}.\end{aligned}\quad (6.15)$$

On combining all the terms together, dropping odd momentum sums, this leads to the symmetrization relation for \hat{H}_3 in the large M limit:

$$\hat{H}_3 = \{ \hat{H}_3 \} - \frac{3C(M+1)}{L} \{ \hat{H}_1 \}.\quad (6.16)$$

Number and momentum variance symmetrization

The number variance is also conserved, as it involves the square of a conserved quantity. For this non-normally ordered case, one must calculate

$$\hat{N}^2 = \sum_k \hat{n}_k^2 + \sum_{k \neq q} \hat{n}_k \hat{n}_q.\quad (6.17)$$

Using the general symmetrization relations given above, one may obtain:

$$\hat{N}^2 = \sum_{k,q} \{ \hat{n}_k \hat{n}_q \} - M \sum_k \{ \hat{n}_k \} + \frac{M(M-1)}{4}.\quad (6.18)$$

Re-arranging this, we then get:

$$\hat{N}^2 = \{ \hat{N}^2 \} - M \{ \hat{N} \} + \frac{M(M-1)}{4}.\quad (6.19)$$

One can also symmetrize the momentum variance, by using the same identities again, to give

$$\hat{P}^2 = \{ \hat{P}^2 \} - \frac{M_2 \Delta k^2}{4}.\quad (6.20)$$

This shows that the apparent momentum variance in a symmetrically ordered measurement has a background term caused by the vacuum fluctuations, which must be subtracted to obtain the true momentum variance.

Position variance symmetrization

The position variance is similar to the number variance, and can be written as a lattice sum over localized number operators \hat{n}_z , using localized creation and annihilation operators with commutators of $1/\Delta z$:

$$\hat{z}^2 = \left(\frac{\Delta z}{N} \right)^2 \left[\sum_z z^2 \hat{n}_z^2 + \sum_{z \neq y} zy \hat{n}_z \hat{n}_y \right].\quad (6.21)$$

Using the general symmetrization relations given above, one may obtain:

$$\{ \hat{z}^2 \} = \left(\frac{\Delta z}{N} \right)^2 \left[\sum zy \{ \hat{n}_y \hat{n}_z \} - \frac{1}{4\Delta z^2} \sum_z z^2 \right].\quad (6.22)$$

Re-arranging this leads to

$$\hat{z}^2 = \{ \hat{z}^2 \} - \frac{1}{4N^2 \Delta z} \int z^2 dz = \{ \hat{z}^2 \} - \frac{M_2 \Delta z^2}{4N^2}.\quad (6.23)$$

This demonstrates that the apparent position variance in a symmetrically ordered measurement also has a background term caused by the vacuum fluctuations that are included in this type of measurement. Just as with the momentum variance, this background contribution must be subtracted from a symmetrized calculation, to obtain the true position variance.

-
- [1] E. P. Wigner, Phys. Rev. **40**, 749 (1932).
[2] P. D. Drummond and A. D. Hardman, Europhysics Letters (EPL) **21**, 279 (1993).
[3] A. I. Streltsov, O. E. Alon, and L. S. Cederbaum, Physical review letters **100**, 130401 (2008).
[4] J. G. Cosme, C. Weiss, and J. Brand, Physical Review A **94**, 043603 (2016).
[5] C. Weiss and L. D. Carr, arXiv preprint arXiv:1612.05545 (2016).
[6] V. A. Yurovsky, B. A. Malomed, R. G. Hulet, and M. Olshani, arXiv preprint arXiv:1706.07114 (2017).
[7] H. B. Thacker, Reviews of Modern Physics **53**, 253 (1981).
[8] B. Davies, Physica A: Statistical Mechanics and its Applications **167**, 433 (1990).
[9] M. Steel, M. K. Olsen, L. I. Plimak, P. D. Drummond, S. Tan, M. J. Collett, D. Walls, and R. Graham, Physical Review A **58**, 4824 (1998).
[10] A. A. Norrie, R. J. Ballagh, and C. W. Gardiner, Phys. Rev. A **73**, 043617 (2006).
[11] W. Kohn, Physical Review **123**, 1242 (1961).
[12] I. Bialynicki-Birula and Z. Bialynicka-Birula, Physical Review A **65**, 063606 (2002).
[13] J. P. Gordon and H. A. Haus, Optics letters **11**, 665 (1986).
[14] P. D. Drummond and W. Man, Opt. Commun. **105**, 99 (1994).
[15] C. Weiss, S. A. Gardiner, and H.-P. Breuer, Physical Review A **91**, 063616 (2015).
[16] C. Weiss, S. L. Cornish, S. A. Gardiner, and H.-P. Breuer, Physical Review A **93**, 013605 (2016).
[17] E. Noether, Transport Theory and Statistical Physics **1**,

- 186 (1971).
- [18] H.-D. Meyer, U. Manthe, and L. S. Cederbaum, *Chemical Physics Letters* **165**, 73 (1990).
- [19] O. E. Alon, A. I. Streltsov, and L. S. Cederbaum, *Phys. Rev. A* **77**, 033613 (2008).
- [20] T. Vaughan, P. Drummond, and G. Leuchs, *Physical Review A* **75**, 033617 (2007).
- [21] M. Kollar, F. A. Wolf, and M. Eckstein, *Physical Review B* **84**, 054304 (2011).
- [22] R. Feynman, *Statistical Mechanics: A Set Of Lectures*, Advanced Books Classics (Avalon Publishing, 1998).
- [23] J.-S. Caux, *Journal of Statistical Mechanics: Theory and Experiment* **2016**, 064006 (2016).
- [24] B. Opanchuk and P. D. Drummond, arXiv preprint arXiv:1708.01013 (2017).
- [25] I. Bloch, J. Dalibard, and W. Zwerger, *Rev. Mod. Phys.* **80**, 885 (2008).
- [26] V. A. Yurovsky, M. Olshanii, and D. S. Weiss, *Advances in Atomic, Molecular, and Optical Physics* **55**, 61 (2008).
- [27] P. Drummond and S. Carter, *JOSA B* **4**, 1565 (1987).
- [28] P. D. Drummond, R. M. Shelby, S. R. Friberg, and Y. Yamamoto, *Nature* **365**, 307 (1993).
- [29] E. H. Lieb and W. Liniger, *Physical Review* **130**, 1605 (1963).
- [30] J. B. McGuire, *Journal of Mathematical Physics* **5**, 622 (1964).
- [31] M. Olshanii, *Physical Review Letters* **81**, 938 (1998).
- [32] K. Kheruntsyan, D. Gangardt, P. Drummond, and G. Shlyapnikov, *Physical Review A* **71**, 053615 (2005).
- [33] S. J. Carter, P. D. Drummond, M. D. Reid, and R. M. Shelby, *Phys. Rev. Lett.* **58**, 1841 (1987).
- [34] J. P. Gordon, *Optics letters* **11**, 662 (1986).
- [35] S. Carter and P. Drummond, *Physical review letters* **67**, 3757 (1991).
- [36] C.-S. Chuu, F. Schreck, T. P. Meyrath, J. Hanssen, G. Price, and M. Raizen, *Physical review letters* **95**, 260403 (2005).
- [37] Y. Lai and H. Haus, *Physical Review A* **40**, 854 (1989).
- [38] R. J. Glauber, *Phys. Rev.* **131**, 2766 (1963).
- [39] M. Rosenbluh and R. M. Shelby, *Phys. Rev. Lett.* **66**, 153 (1991).
- [40] J. F. Corney, J. Heersink, R. Dong, V. Josse, P. D. Drummond, G. Leuchs, and U. L. Andersen, *Phys. Rev. A* **78**, 023831 (2008).
- [41] H. Thacker, *Physical Review D* **17**, 1031 (1978).
- [42] S. Jin, C. D. Levermore, and D. W. McLaughlin, *Communications on Pure and Applied Mathematics* **52**, 613 (1999).
- [43] M. Rigol, V. Dunjko, V. Yurovsky, and M. Olshanii, *Physical review letters* **98**, 050405 (2007).
- [44] F. Essler, G. Mussardo, and M. Panfil, *Physical Review A* **91**, 051602 (2015).
- [45] A. Shabat and V. Zakharov, *Soviet physics JETP* **34**, 62 (1972).
- [46] E. Gutkin, in *Annales de l'Institut Henri Poincaré (C) Non Linear Analysis*, Vol. 2 (Elsevier, 1985) pp. 67–74.
- [47] R. J. Glauber, *Physical Review* **130**, 2529 (1963).
- [48] P. D. Drummond and C. W. Gardiner, *J. Phys. A: Math. Gen.* **13**, 2353 (1980).
- [49] J. F. Corney, P. D. Drummond, J. Heersink, V. Josse, G. Leuchs, and U. L. Andersen, *Phys. Rev. Lett.* **97**, 023606 (2006).
- [50] B. Opanchuk and P. D. Drummond, *Journal of Mathematical Physics* **54**, 042107 (2013).
- [51] L. D. Faddeev and L. Takhtajan, *Hamiltonian methods in the theory of solitons* (Springer Science & Business Media, 2007).
- [52] J. Moyal, *Proceedings of the Cambridge Philosophical Society* **45**, 99 (1949).
- [53] R. Graham, *Quantum Statistics in Optics and Solid-State Physics*, edited by G. Hohler, Vol. 66 (Springer, New York, 1973) p. 1.
- [54] P. Kinsler, M. Fernée, and P. Drummond, *Physical Review A* **48**, 3310 (1993).
- [55] P. Kinsler, *Phys. Rev. A* **53**, 2000 (1996).
- [56] P. Wai, C. R. Menyuk, Y. Lee, and H. Chen, *Optics letters* **11**, 464 (1986).
- [57] S. Kiesewetter, R. Polkinghorne, B. Opanchuk, and P. D. Drummond, *SoftwareX* **5**, 12 (2016).
- [58] B. Opanchuk, “Reikna: a pure Python GPGPU library,” <http://reikna.publicfields.net> (2014).
- [59] B. M. Caradoc-Davies, *Vortex dynamics in Bose-Einstein condensates*, Ph.D. thesis (2000).
- [60] A. Sinatra, C. Lobo, and Y. Castin, *Journal of Physics B: Atomic, Molecular and Optical Physics* **35**, 3599 (2002), arXiv:condmat/0201217.
- [61] P. P. Deuar and P. D. Drummond, *Phys. Rev. Lett.* **98**, 120402 (2007).
- [62] P. D. Drummond and S. Chaturvedi, *Physica Scripta* **91**, 073007 (2016).